PERGAMON

Journal of Structural Geology 23 (2001) 675–691

JOURNAL OF STRUCTURAL GEOLOGY

www.elsevier.nl/locate/jstrugeo

3-D rock salt fabrics in a shear zone (Súria Anticline, South-Pyrenees)

L. Miralles[a,*], M. Sans[b], S. Galí[c], P. Santanach[b]

[a]*L.I.F.S. Dept. Geoquímica, Petrologia i Prospecció Geològica, Universitat de Barcelona, Barcelona, Spain*
[b]*Dept. Geodinàmica i Geofísica, Universitat de Barcelona, Barcelona, Spain*
[c]*Dept. Cristal.lografia, Mineralogia i Dipòsits Minerals, Universitat de Barcelona, Barcelona, Spain*

Received 8 June 1999; accepted 15 August 2000

Abstract

The internal geometry of the evaporitic horizons serves as a good indicator of their large-scale behaviour. However, the determination of the strain ellipsoid inside the deformed salt bodies can often be difficult. Moreover, the relationship between the bulk strain ellipsoid and the grain shape ellipsoid is not straightforward, and two parameters, orientation and the dimension of the grain shape ellipsoid, need evaluation. The grain shape ellipsoid is not an indicator of the dimensions of the bulk strain ellipsoid. The increase in shear strain led initially to a growth in grain volume followed by a reduction to a value near the original volume, specifically due to the long axis change. The orientation of the grain shape ellipsoid runs parallel to that of the strain ellipsoid after a certain amount of deformation. These changes were accompanied by the growth of a new tectonically oriented grain population. The rapid spatial changes in morphology contrast with the constant and strong {100} texture. The intracrystalline deformation mechanism consistent with this texture is the $\{110\}\langle 1\bar{1}0\rangle$ slip system. Nevertheless, a mechanism such as fluid assisted grain boundary migration might have also taken place to account for the grain volume changes.

1. Introduction

Interest in saline formations has increased recently as their suitability for nuclear and toxic waste disposal has been established. Consequently, much research has been conducted with natural and synthetic rock salt samples deformed under laboratory conditions, in order to determine their mechanical behaviour and deformation mechanisms. Most work has been performed on the testing of salt monocrystals (Carter and Heard, 1970; Wanten et al., 1993), synthetic fine grained (1 mm) aggregates of rock salt (Spiers et al., 1986) and natural rock salt (domal salt) of large grain size (2–3 cm) (Carter and Hansen, 1983). A range of deformation conditions at various temperatures have been examined, including extrusion (Skrotzki and Welch, 1983), shear (Knapp et al., 1987; Ross et al., 1987; Chester, 1988; Fransen, 1993), creep (Carter and Hansen, 1983; Spiers et al., 1986; Urai et al., 1986), uniaxial (Fransen, 1993) and triaxial (Kern, 1977). All of them have improved our knowledge of rock salt rheology and its mechanical properties under the tested experimental conditions. From these experiments two main deformation mechanisms have been reported: (1) dislocation controlled creep, including solid state recrystallization (Carter and Hansen, 1983; Wawersik and Zeuch, 1986) and, (2) fluid assisted grain boundary migration (or solution–precipitation processes), considered as a dynamic mechanism and as producing static recrystallisation. This mechanism involves dissolution in the high mean normal stress direction, transport through the grain boundaries and precipitation in the low mean normal stress direction (Urai et al., 1986; Spiers et al., 1990). Studies conducted on naturally deformed rock salt show microstructural evidence for the operation of solution–precipitation processes (Urai et al., 1986, 1987) as well as the presence of microstructures characteristic of intracrystalline dislocation mechanisms (Carter and Hansen, 1983).

Salt structures rarely form outcrops that can be mapped and studied. Therefore, most macroscale analyses rely on imaging the salt structures and contouring their external shape by geophysical methods (Peel et al., 1995; Pinto and Casas, 1996; Koyi, 1998), though this means little is known about their internal structure. One exception are a small number of studies carried out in salt mines (Muehlberger and Clabaugh, 1968; Kupfer, 1968; Burliga, 1996; Sans et al., 1996a). None of these, however, shows a complete study from the regional framework to the internal structure of the salt bodies and its relationship to the rock salt fabric. In contrast to the abundance of studies conducted

* Corresponding author.
E-mail address: lourdes@naturageo.ub.es (L. Miralles).

0191-8141/01/$ - see front matter © 2001 Elsevier Science Ltd. All rights reserved.
PII: S0191-8141(00)00138-3

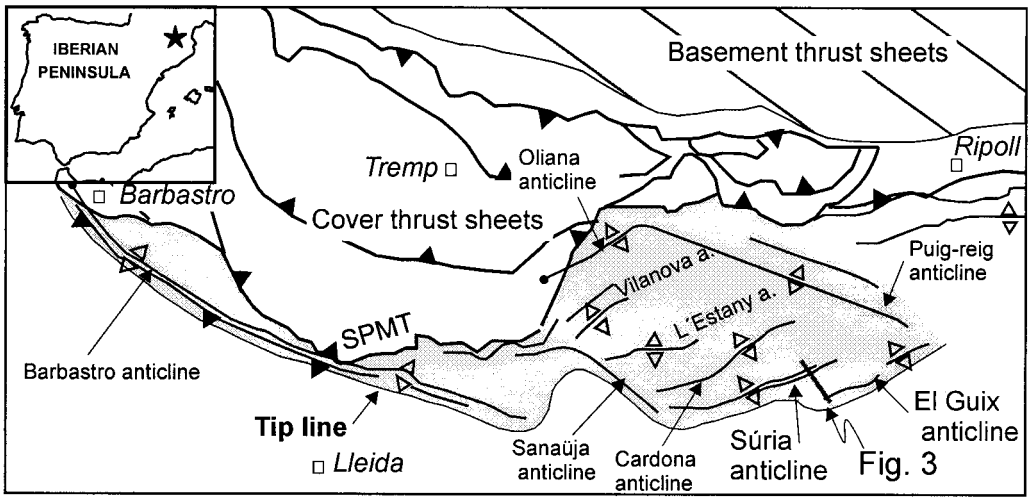

Fig. 1. The deformed south Pyrenean foreland has different fold trends which correspond to three detachments (evaporitic formations) at depth (modified from Sans et al., 1996b). See location of the cross section shown in Fig. 3.

on laboratory deformed rock salt samples, very few attempts have been made to study naturally deformed rock salt, be it by lithostatic or tectonic stresses. The difficulty in studying and interpreting these fabrics lies in the rapid recrystallization of rock salt, which tends to increase grain size and causes the original fabric to disappear (Talbot and Jackson, 1987). Although some studies have been carried out in core samples (Carter and Hansen, 1983; Larsen and Lagoni, 1984) and isolated outcrops (Muehlberger and Clabaugh, 1968; according to Brokmeier, 1983 in Kern and Richter, 1985; Ertel et al., 1987), they have not been precisely located in the structural framework so as to provide evidences of the mesoscale and macroscale structures which might have had a bearing on the fabrics of the samples selected.

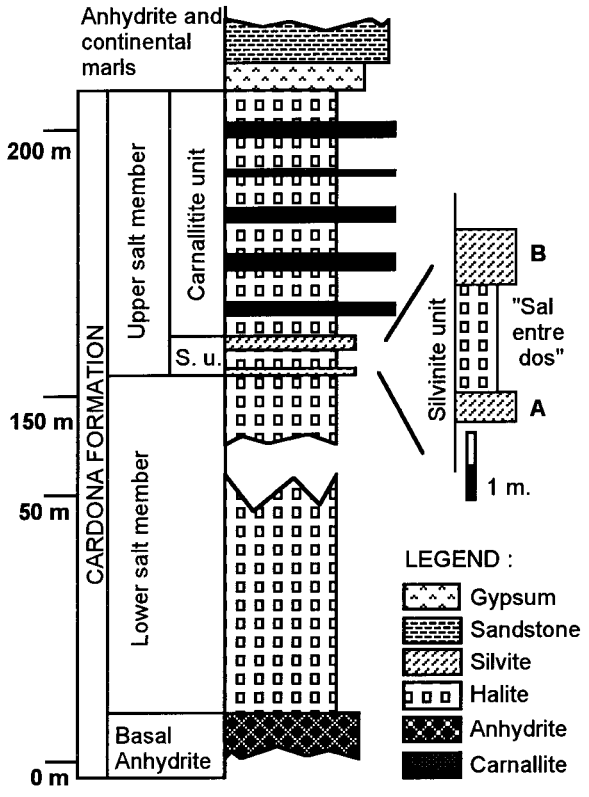

Fig. 2. Stratigraphic section of the Cardona Formation and the deformed sedimentary pile overlying it. S.u. stands for the lower Sylvinite unit, A and B stand for the enriched potassic layers, and "sal entre dos" is alternating layers of centimetre-scale halite cycles and millimetre-scale dark clay.

Our purpose here is to establish a link between strain and fabric changes. To do this, we set out to determine the evolution of the strain ellipsoid and to quantify the variations in the morphological and crystallographic fabrics in a naturally deformed thin bed of fine grain size.

The structure selected for this study was a shear zone affecting the limb of a metre-scale fold. This type of shear zone has been described in detail at the regional tectonic scale (Sans et al., 1996a). The strain ellipsoid was determined in each position at which the shear zone had been sampled for fabric analysis. The morphological and crystallographic fabric changes were quantified and the relationship between morphological, crystallographic fabrics and strain is discussed. Moreover, the rock salt samples studied here had a small grain size (from tenths of microns to 2 mm) which permits its comparison with salt samples used for experimental work. In addition, we suggest that halite grains should be treated as a 3-D body as wrong conclusions might be drawn, depending on the 2-D section chosen, when a dominant grain shape orientation is present. Finally, a coherent deformation mechanism is proposed.

2. Geological setting

The geometry and structure of the southeastern Pyrenean foreland is controlled by the presence of three Paleogene evaporitic formations at depth (Vergés et al., 1992). From north to south and from bottom to top, these evaporitic

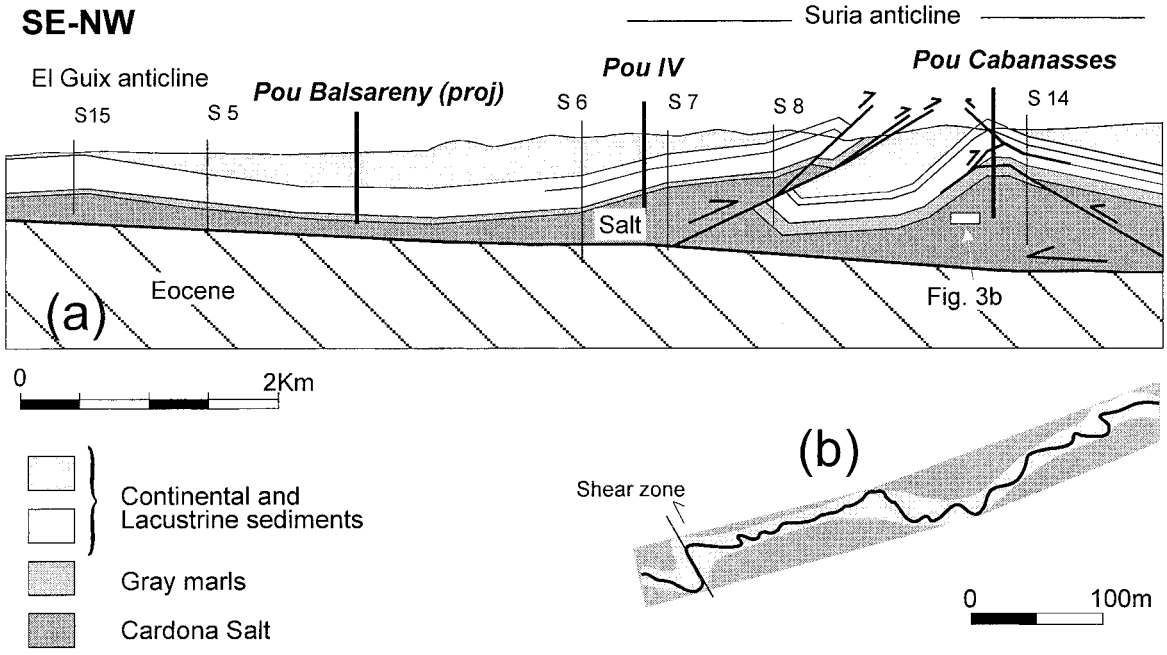

Fig. 3. (a) Cross-section of the two frontal most structures of the south Pyrenean foreland. The synclines are flat-bottomed and wide whereas the anticlines are complex and narrow. They show no dominant vergence and the development of fish-tail structures and frontal thrust-wedges at different stratigraphic levels. The Súria anticline is a double-structure with a north-directed fault-related-fold to the south and a south-directed fold in the north. The shear zone studied here is located on the southern limb of the northern anticline (Cabanasses anticline). Pou Balsareny is projected from 6 km to the east. (b) Simplified section of the potash layers. The black trace shows the geometry of the tens of metres folds, and light grey represents the enveloping surface of these folds which is folded in hundreds of metres folds.

formations are the Beuda, Cardona and Barbastro formations. At the surface (Fig. 1), each evaporitic formation is characterised by: (1) folds of different trends (Vergés et al., 1992), and (2) the development of a thrust wedge coinciding with their boundaries (Sans et al., 1996b). The basal detachment, south of the emergent frontal thrust, has a flat and ramp geometry. Flats lie within the evaporitic formations and ramps develop at their sedimentary limits (Sans et al., 1996b; Sans, 1999). The detachment in the Cardona Formation is the most effective and, at the surface, it coincides with NE–SW trending folds. These folds are, from south to north, El Guix, Súria, Cardona, L'Estany and Vilanova de l'Aguda (Fig. 1).

The Cardona Formation has a sedimentary salt thickness of 300 m at the centre of the basin (Pueyo, 1975). Three members (Fig. 2) can be distinguished: (1) a basal anhydrite, (2) a lower massive salt member and, (3) an upper banded salt member bearing potash salts. The basal anhydrite member is 4–5 metres thick and laminated. It consists of aggregates of elongated prismatic crystals parallel to bedding, interfingering with millimetre layers of micritic carbonate. The lower massive salt member is 130–200 m thick. It consists of white and grey decimetre-scale banded halite (Busquets et al., 1985). The grey bands result from the sedimentary accumulation of abundant hopper crystals (1–2 cm) and diffuse clay. The clear bands consist of transparent grains or hopper crystals that are smaller than those in the grey bands. The upper banded salt member is 50–100 m thick (Pueyo, 1975; Ayora et al., 1995). This member consists of two units: (a) the lower sylvinite unit (extensively mined in Súria and Sallent), and (b) the upper carnallitite unit. The sylvinite unit includes two enriched sylvinite layers (known as A and B layers) separated by alternating layers, 2 m thick, of centimetre- and millimetre-scale cycles of halite and dark clay, which are known as "sal entre dos". These halite cycles, composed of small (1 mm) clear halite grains, locally show a grain size gradation. The grains can be elongated and include small cubic or elongated hopper crystals that are related to the enriched clay layers (Rosell and Pueyo, 1997). The upper carnallitite unit consists of 40–80 m of alternating beds of carnallite (10 cm to 2 m), thinner halite and clay horizons. The carnallite beds are red and coarse grained, usually brecciated with irregular fragments of anhedral red crystals of carnallite in a pink matrix.

Underground mining activity, which is targeted at the potash layers, greatly facilitates the study of the internal structure of the Cardona Formation. Mapping and cross-section analysis of the exploitation area show structures of different magnitudes (Sans et al., 1996a). The larger structures are asymmetric folds (of almost 100 m in wavelenght) (Fig. 3b) coherent with their location with respect to the kilometre-scale folds which outcrop at the surface. On the other hand, the metre to tens of metres structures consist mainly of south-vergence folds, independently of their

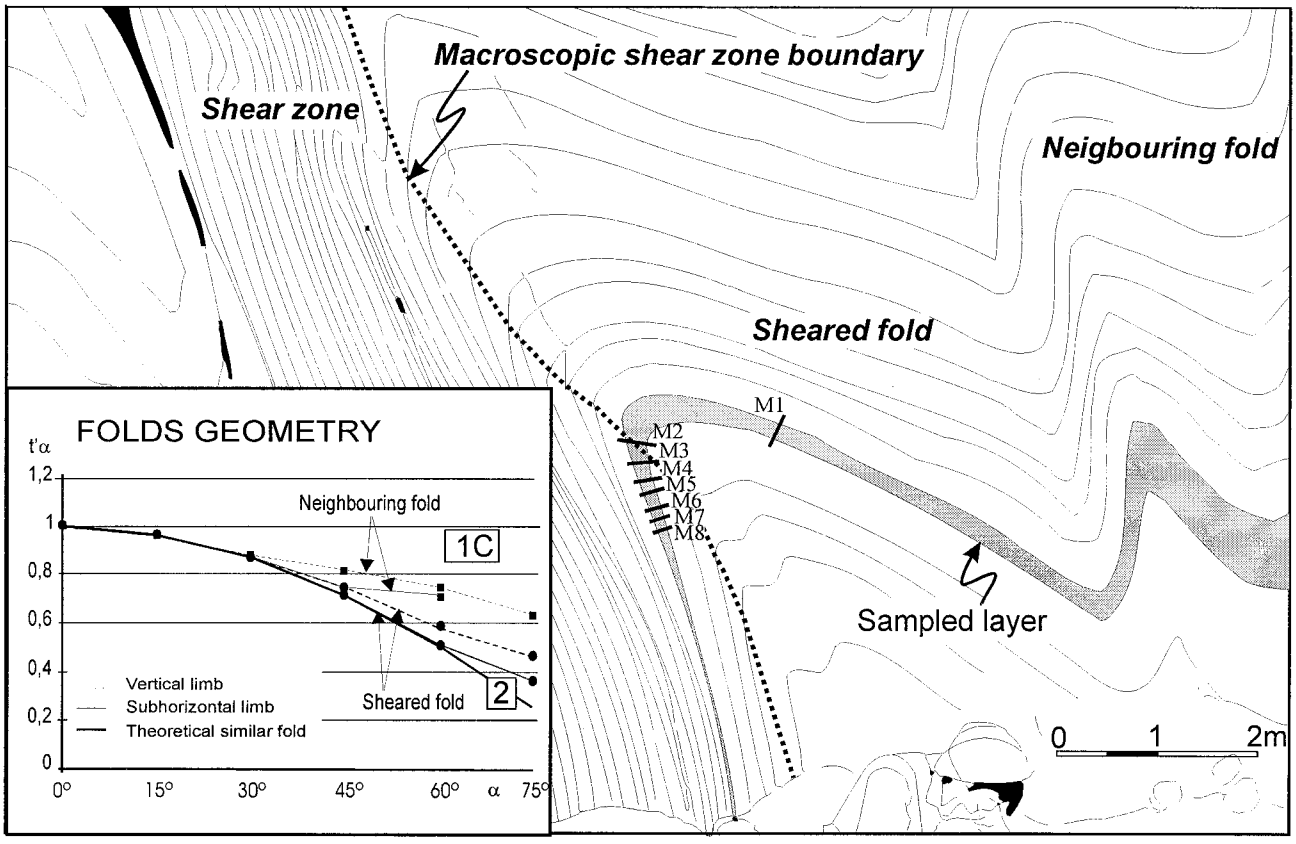

Fig. 4. Sketch of the shear zone outcrop in the mine gallery. Sample 1 was taken from the northern limb and samples 2 to 8 were from the vertical limb. The inset shows the geometry of the folds in a $t'\alpha$-α plot.

location with respect to the larger structure. These observations, together with the presence of boudins and multiple top-south shear, suggest a generalised top to the south shear of the whole detachment horizon prior to the formation of the kilometre-scale folds (Sans et al., 1996a). The studied shear zone is located in the sheared limb of a metre-scale fold located in the Cabanasses mine (Fig. 4).

3. Method

To analyse the relationship between the strain ellipsoid and changes in the morphological and crystallographic fabrics, a detailed macroscopic and microscopic study was carried out. First, there is a good control on the relationship of the sampled structure with the regional framework and tectonic transport direction. Second, at a local scale, the calculation of the mesoscopic strain ellipsoid for each sample in the shear zone was carried out. Third, powerful quantitative techniques or the analysis of the morphological and crystallographic changes in all the samples were used. These results were integrated in a 3-D calculation of the grain shape ellipsoid, which enabled a good comparison to be made with the patterns of the crystallographic orientations and the strain ellipsoid.

3.1. Fold geometry and determination of the finite strain ellipsoid

Fold geometry was determined by the dip isogons and thickness variation methods (Ramsay, 1967). Not only was the sheared fold analysed but also the neighbouring folds, which provided a geometric reference when comparing the changes undergone by the sheared limb.

Shear strain values, in the studied shear zone, have been calculated according to Carreras (1975). This method was developed to calculate shear strain in a shear zone, which presented a previous planar heterogeneity (e.g. cleavage, bedding). It assumes that two parallel planes limit the shear zone, between which, shear is homogeneous and that there is only displacement in one direction. The analytical analysis is based on the examination of the displacement of a reference surface between the two planes that limit the shear zone and calculates the variation in orientation of this for different values of displacement. The data needed to use the simplified graphical method proposed by Carreras (1975) are measurements, which are easily obtained from the field. These data are (1) the angle between the reference surface before deformation and the shear plane, and the angle between the reference surfaces after deformation and the shear plane (α and α_0 respectively)

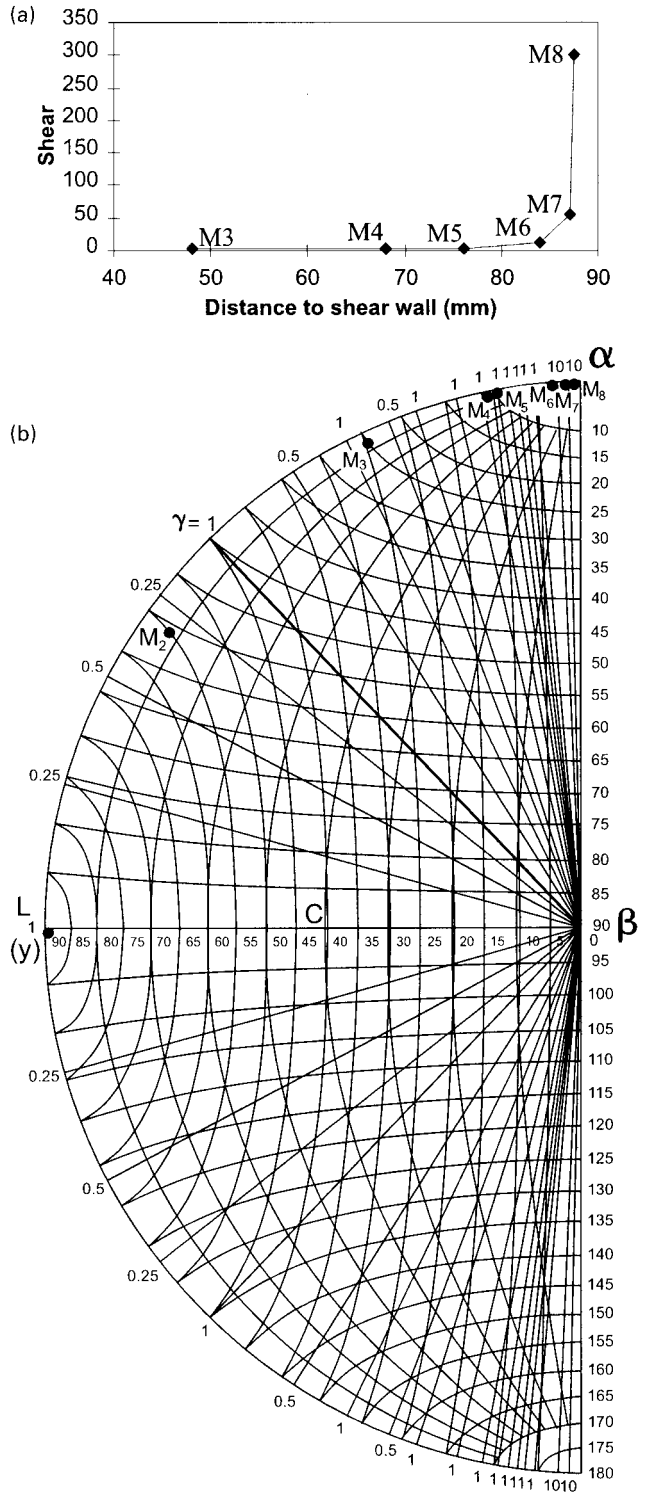

Fig. 5. (a) Distance to shear wall/shear strain graph shows rapid increase in the shear values away from the shear zone boundary. (b) All samples plot in the same deformation path in a deformation-path plot based on Carreras (1975). See text for explanation.

and (2) the angles between the undeformed reference surfaces and the motion direction, and the deformed reference surfaces with the motion direction (β and β_0 respectively). The graphical method allows visualising (Fig. 5) the deformation paths of a surface as deformation values increase. It consists of a semi-circle in which it is possible to represent all the orientations of the reference plane with respect to the shear plane, which is represented in the E–W radius. The minor circles represent the isogons of the α and β angles, 0 to 180° for α and 0 to 90° for β. In this graph, the location of the reference surface is at the intersection of the isogons of the calculated α and β values. The thick radial lines represent lines of equal increment of γ and the value of each increment is shown on the outside of the semi-circle. Finally, the maximum circles show the path of the reference surface as it deforms. In the studied example, bedding is taken as the reference surface and it can be measured outside the shear zone as undeformed and inside the shear zone as deformed. Measurements in several positions inside the shear zone give different angular relationship between the deformed reference surface and the shear plane. The principal finite strain axes and the ellipticity of strain ellipsoid in the outcrop section were calculated from the shear values according to the expressions in Ramsay and Hubert (1987), p. 15 and 599. The ellipticity of the other two sections and the value of $1 + e_2$ were calculated from the results of the previous expressions and assuming plane strain ($Y = 1$).

3.2. Sampling

Sampling sites were selected on shear zones and folds which were considered representative of the structural style attained by the Cardona Formation in the Súria northern anticline. These structures could be followed for several tens to hundreds of meters and were represented in the structural maps and sections of the exploitation area (Súria, 1994, internal report; Sans et al., 1996b). In this paper, we present the results from one of the six sites sampled between the two layers of sylvinite at the "sal entre dos" level through the Súria northern anticline. At this site, eight oriented samples were taken at different correlative positions in the shear zone. From the oriented samples, three mutually perpendicular thin sections were cut and labelled in accordance with the stratigraphic coordinate system ***ac**, ***bc**, ***ab** where * was the number of the sample. In this system, + **b** axis is the dip direction, +**c** axis is the perpendicular to the stratification plane pointing to the top of the layer and +**a** axis is perpendicular to both. On these sections, the measurements of the salt fabrics, either the morphological parameter or the crystallographic orientations have been performed.

Gentle, low speed procedures were applied to the rock salt samples to obtain the thin sections without inducing damage by sample manipulation. Moreover, samples were stored and manipulated in low humidity conditions to prevent grain boundary dissolution, damage, or any structural change (Miralles, 1999).

Water content was determined by termogravimetry since this technique allows one to quantify the amount of water

and to discern the different types of water present (e.g. trapped in fluid inclusions, adsorbed at the grain boundaries or compositional water of hydrated minerals). The exhaustive working conditions and the corrections made are described elsewhere (de las Cuevas and Pueyo, 1995).

3.3. Quantitative morphological analysis of the salt grains

The quantification of the morphological parameters of the salt grains was carried out using a conventional image analysis of the grain boundary network performed on the 2-D sections from which the 3-D results were calculated. The images of the grain boundary network (three sections, mutually perpendicular, for each sample studied) were obtained either by a video camera or a drawing tube adapted to the petrographic stereomicroscope (from 2.5 to 25×). The illumination conditions comprised a combination of reflected and transmitted light, in order to ensure a complementary image and a better resolution of those boundaries badly oriented with respect to the illumination focus. Afterwards, the image of the grain boundary network was scanned (100 dpi) and the image (580 × 780 pixels) was processed using the IMAT program (Serveis Cientificotècnics, Barcelona University). With this program, the Area (A), Perimeter (P), Long axis (L), Short axis (S) and the angle Phi were measured for each grain. The long axis is the line between the two most distant points in the grain, which crosses the centroid, considering the grain as a rigid body of uniform density. The short axis lies perpendicular to the long axis and crosses the centroid. These variables were measured as absolute dimensions and, therefore, data was obtained in mm and mm^2 (in the case of the area). The angle Phi is the angle between the long axes and a reference line. For sections **ab** and **ac** the reference is (+) **a,** whereas for section **bc** the reference is (+) **b** axis of the stratigraphic coordinate system. A stereological correction was applied to the data measured in each section because the sections studied were apparent with respect to the sections crossing the centroid of the grains in 3-D. The factor applied is $d_{corrected} = (4/\pi)\ d_{apparent}$; $d_{corrected}$ stands for corrected axis and $d_{apparent}$ stands for the measured axis which is, in fact, an apparent measurement. This factor is the same used by other authors (Cashman and Marsh, 1988).

From the measured data, the form factor L/S defined by the ratio between the Long axis (L) and the Short axis (S) which were measured as absolute dimensions, and a named ellipse form factor $(E.F.F.) = 2LP/(\pi L^2 + 4A)$ calculated according to the ellipse formula $A = \pi(L/2)(S/2)$ (Larsen and Lagoni, 1984) were calculated. In fact, the E.F.F. is a measure of the ratio of the perimeter of an object to the perimeter of an ellipse of the same area. Therefore, this form factor also gives information on the degree of rugosity of the grain boundaries. Mean grain size was also calculated as the diameter of a circle with an area equal to the measured area of the salt grains.

3.4. Morphological analysis in 2-D

3.4.1. Univariant analysis

In most of the sections studied more than 300 individual salt grains were measured. The results of the different measured and calculated morphological parameters were statistically treated to determine the number of populations present and to obtain the mean value for each variable and sample. Grains were not treated individually. In order to approximate normal distributions, the data sets had to be transformed to logarithmic (area and perimeter), to the square-root (long and short axis), and to reciprocal (L/S). The Kolgomorov–Smirnov test was applied and the critical value $\alpha = 0.05$ in a two-tailed test was taken as a boundary to reject the hypothesis that samples follow a normally distributed population (Davis, 1986). For the form factor E.F.F., the mean values and standard deviation were obtained from the raw data, since none of the usual transformations could approximate the data to a normal, chi square or gamma distribution. In the case of angular values, the raw data were also used to obtain the mean value and to check for the presence of more than one main orientation. From the comparison between the theoretical normal distribution and the obtained grain population (after transformation), the presence of more than one population could be discerned.

3.4.2. Bivariant analysis. The L/S / Phi method

The L/S / Phi method contrasts the ratio L/S against the angle Phi. In this paper, the L/S ratio and associated values were calculated by the GRFRFP program (D. Durney, 1995, University of Barcelona) and plotted according to the projection system of Elliot (1970) which is based on a ln-L/S / 2 Phi polar plot. The program GRFRFP calculates the mean ellipticity of a set of ellipses by iterative retrodeformation of this set to an isotropic distribution (with a zero ln (L/S)/2).

3.5. Morphological analysis in 3-D. The grain shape ellipsoids

The 3-D representative shape of the grains was reduced to a unique triaxial ellipsoid, which was characteristic of each sample. The ellipsoid was defined by six independent parameters, which are the mean values obtained from the statistic treatment of the measurements performed on the 2-D sections. For an exact solution, two sections are sufficient to determine the ellipsoid. However, in the present case, for each sample, estimated L, S and Phi values of the three perpendicular sections were used to build a linear system of nine equations with six unknowns. The excess number of equations with respect to the sought parameters allows the least square method to be applied. The solution obtained by least squares is unique. However, the coefficients of the representative quadric obtained could give a surface different from an ellipsoid. In this case, more

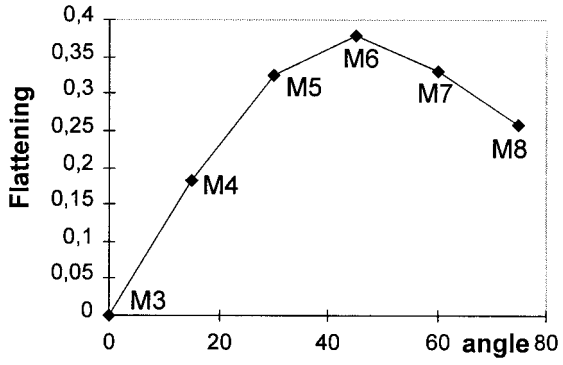

Fig. 6. The flattening component is not constant across the shear zone, which indicates that there is no homogeneous strain superimposed on the shear deformation.

sections with a different orientation should be added to the least squares procedures to obtain a good result. In any case, diagonalization of the resulting symmetric matrix gives six values, which consist of the coefficients of the ellipsoid characteristic for each sample. In other words, the absolute lengths and orientations of the three axes of the ellipsoid are obtained.

3.6. Crystallographic grain orientation. Texture

The full crystal orientation of each grain was measured in a U-Stage. Crystals in thin section were cleaved by mechanical shock along {100} planes. At least two perpendicular {100} planes had to be present to permit the measurement of the complete crystal orientation. The thin sections measured correspond, in all samples, to the **bc** section of the stratigraphic coordinate system. An area of 16×16 mm was scanned and a measurement was taken every 1 mm^2, giving a maximum of 256 measurements. Orientation angles of every square millimetre measured on the U-stage were readily transformed to the Euler angles. These angles allow the representation of a discrete orientation distribution function (ODF). The ODF contains all the information regarding crystallographic orientation. In particular, any desired pole figure can be obtained by calculating the polar coordinates of a given {hkl} family plane, for every square millimetre.

4. Results and discussion

4.1. Shear zone, fold description and strain calculation

In the Cardona Formation, shear zones are mainly located in two settings: (1) in the lithologic contact between the carnallite and halite layers and, (2) in the stretched and inverted limbs of the asymmetric south-vergent folds. The shear zone selected is located on the southern limb of the northern and south-vergent kilometre-scale fold of the Súria double anticline (Fig. 3), in the stratigraphic level of "sal entre dos" (Fig. 2). This shear zone belongs to the second setting and is related to a system of metre-scale folds with wavelength from 0.5 m to 5 m and amplitudes in the same order of magnitude. These folds (Fig. 4) are asymmetric and mainly south vergent (Sans et al., 1996a). They have straight limbs and, narrow and rounded hinges (interlimb angle ranging from 74° to 86°). The mean orientation of the folds' axes is N075E and remain largely horizontal (Sans et al., 1996a). These metre-scale folds have millimetre-scale parasitic folds developed in the clay beds, only present in the subhorizontal limbs. The strike of the shear zone documented in this paper has a N068E orientation, lies subparallel to the fold axis and dips 64° to the north. This orientation is consistent with previous reports of the shear zones and it is coherent with a reverse motion within the detachment level (Sans et al., 1996a).

The lack of macroscopic kinematic indicators in the shear plane does not permit one to infer the motion direction by direct observation. However, an assumption of a motion direction as a pure reverse shear with a top to 158° N slip direction would be compatible with the constant 070N strike of the folds in the study area (Sans et al., 1996a,b), the top to 160–170° N transport direction inferred from the analysis of kinematic indicators in the overburden (Sans, 1999) and the presence in the clay layers in the shear zone of subhorizontal rectangular boudins of 1–1.5 cm with opening spaces of 2–3 mm filled with halite crystals. The shear zone is 1.8 m wide and represents a thinning of 65% with respect to the northern limb of the related anticline, which is considered as not being deformed by the shear zone. From the thinning value measured, a slip of 7 m has been calculated.

The geometric analysis of the folds neighbouring the shear zone shows class 1C for both limbs according to the thickness variation plot $t'\alpha$-α (Fig. 4). This classification agrees with the convergent geometry towards the core of the anticline of the dip isogons. In contrast, the fold affected by the shear zone shows a different classification for both limbs. The northern subhorizontal limb lies in the 1C class field in the thickness-variation plot. The southern, overturned, sheared limb follows the class 2 curve with a good fit except for the last measurement at 75° which lies above the curve, in the 1C class. The dip isogons show the same result: convergent dip isogons for the northern limb and parallel isogons for the sheared limb, confirming classes 1C and 2, respectively. The good fit of the geometry of the sheared limb with a class 2 curve might be interpreted as a result of a deformation achieved by axial planar simple shear alone. Nevertheless, class 2 folds can also develop from class 1C folds, which have undergone a homogenous flattening. If this were the case, the coaxial flattening component (a) would be constant throughout the shear zone. The component $\boldsymbol{a}$ is calculated as

$$a = \sin\alpha_0 t_i / \sin\alpha_i t_0 \quad (1)$$

where t_0 is the initial thickness and t_i the final thickness perpendicular to bedding and α_0 and α_i are the angle with

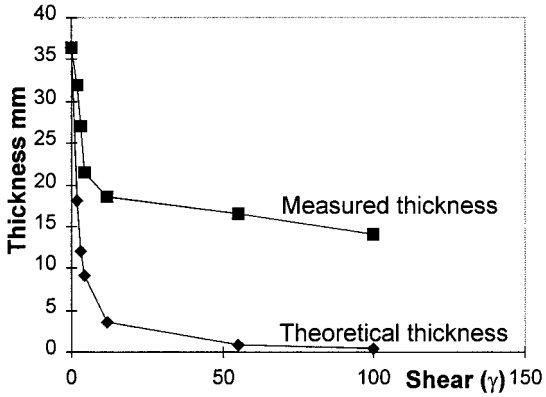

Fig. 7. Comparison between a theoretical thinning of the sampled layer by simple shear and the measured thinning.

the shear zone before and after deformation (Carreras and García, 1982). The variation of the component ***a*** through the shear zone (Fig. 6) indicates that there is no homogeneous strain superimposed on the simple shear model.

To corroborate, the simple shear model, we compared the thinning of the beds affected by a theoretical simple shear model with the real thinning measured in the hand sample (Fig. 7). The thinning of the bed as it enters the shear zone is related to the shear component by the following expressions

$$\tan\beta_1 = \tan\beta/(1 + \tan\beta\tan\alpha) \quad (2)$$

$$h_1 = h\sin\beta_1/\sin\beta \quad (3)$$

where β and β_1 are the initial and final angles between bedding and the shear walls, α is the shear angle, and h and h_1 are the initial and final thicknesses of the layer.

Both curves show the same trend, starting from an initial thickness of 36 mm, but whereas the theoretical curve tends to zero, the measured curve tends to a thickness of 14 mm. This difference indicates that although the final geometry of the shear limb can be explained by simple shear alone, it probably results from a more complex deformation that

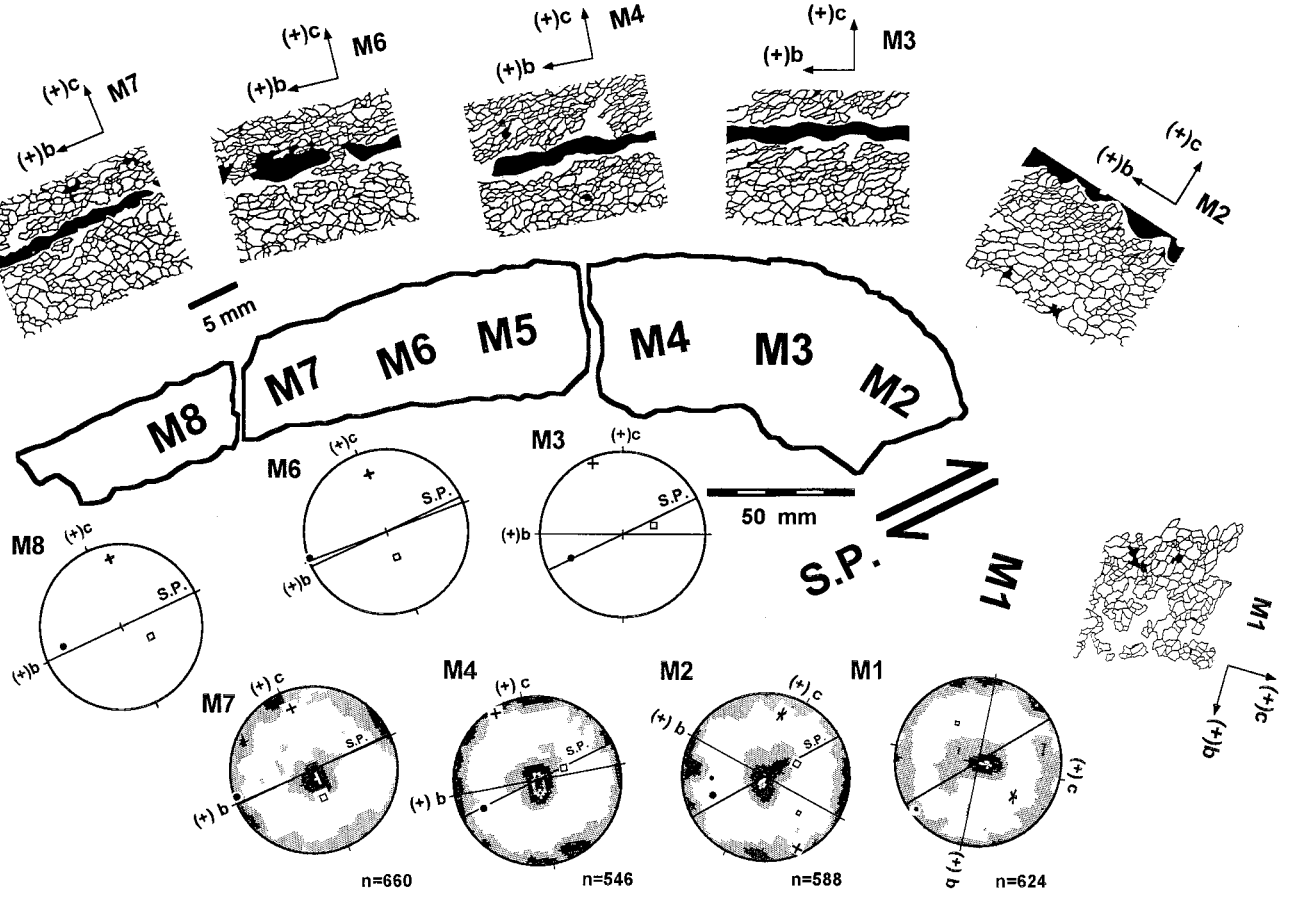

Fig. 8. Sketch of the sampled layer and detailed location of the samples analysed to determine their crystallographic and morphological fabric (see Fig. 4 for general location). This figure is a 2-D section according to the bc plane of the statigraphic coordinate system and has been chosen to illustrate the main findings as it is the most sensitive to morphological change. Images of the grain boundary network for different samples as well as their mobile reference axis (stratigraphic coordinate system) are plotted. The shear plane (S.P.) is plotted as a great circle. The grain shape ellipsoid orientations and textures are plotted in the lower hemisphere equal area projection, on the bc projection plane. The circles represent the orientation of the long axis, the squares the intermediate axis and the star and the cross the short axis. The star, the small circle and square indicate the initial orientation. The larger symbols and the cross indicate the orientation of the new population (see text for explanation). Textures are shown as {100} pole density figures of 1% of 1% area on the bc plane. The same projection plane has been used for morphological and crystallographic parameters to facilitate comparison (see text for explanation).

Table 1
Geometrical and calculated parameters of the shear zone at the locations sampled for the fabrics (morphology and crystallography) study. Angle (θ) between bedding and the shear zone walls, (γ) shear angle, X, Y and Z are the strain axes, and Rxz and Ryz, the ellipticity of the strain ellipsoid in these sections.

Sample	θ	γ	X	Z	Y	Rxz	Ryz
M2	54		–	–	–	–	–
M3	29	1.6	2	0.5	1	4.2	2
M4	19	2.9	3.2	0.3	1	10.3	3.2
M5	15	4.1	4.3	0.2	1	18.5	4.3
M6	7	12	12.1	0.1	1	147.2	12.1
M7	3	55	55	0	1	3031.4	55
M8	0	8	8	0	1	8	8

should include simple shear, flattening and a rotational component through time.

In order to calculate the finite strain ellipsoid in different positions in the shear zone we assumed plane strain deformation. This assumption seemed reasonable from the observations in the overburden and the mesostructure orientation in the salt layer. A nascent cleavage is present perpendicular to bedding regardless of bedding orientation and dip (Sans and Vergés, 1995) giving evidence of deformation prior to folding in which the *Z* axis of the strain ellipsoid was contained on the bedding plane and perpendicular to the *XY* plane defined by cleavage (Sans, 1999). The detachment of the studied folds at less than 2.5 km from the synorogenic surface suggests maximum elongation according to the vertical *X* axis of the strain ellipsoid and no elongation along the *Y* axis which is confined. In the salt horizon the constant fold trend, the lack of extensional structures (e.g. boudins) in a direction oblique or perpendicular to the fold axes and the fact that the studied example is in the central part of a larger fold and not in its terminations suggest that plane strain is a reasonable assumption for the studied structure. Therefore, in the studied example, the *Y* strain direction is parallel to the folds' axis and the outcrop corresponds to the *XZ* section. The strain ellipsoid was calculated in seven different positions with increasing

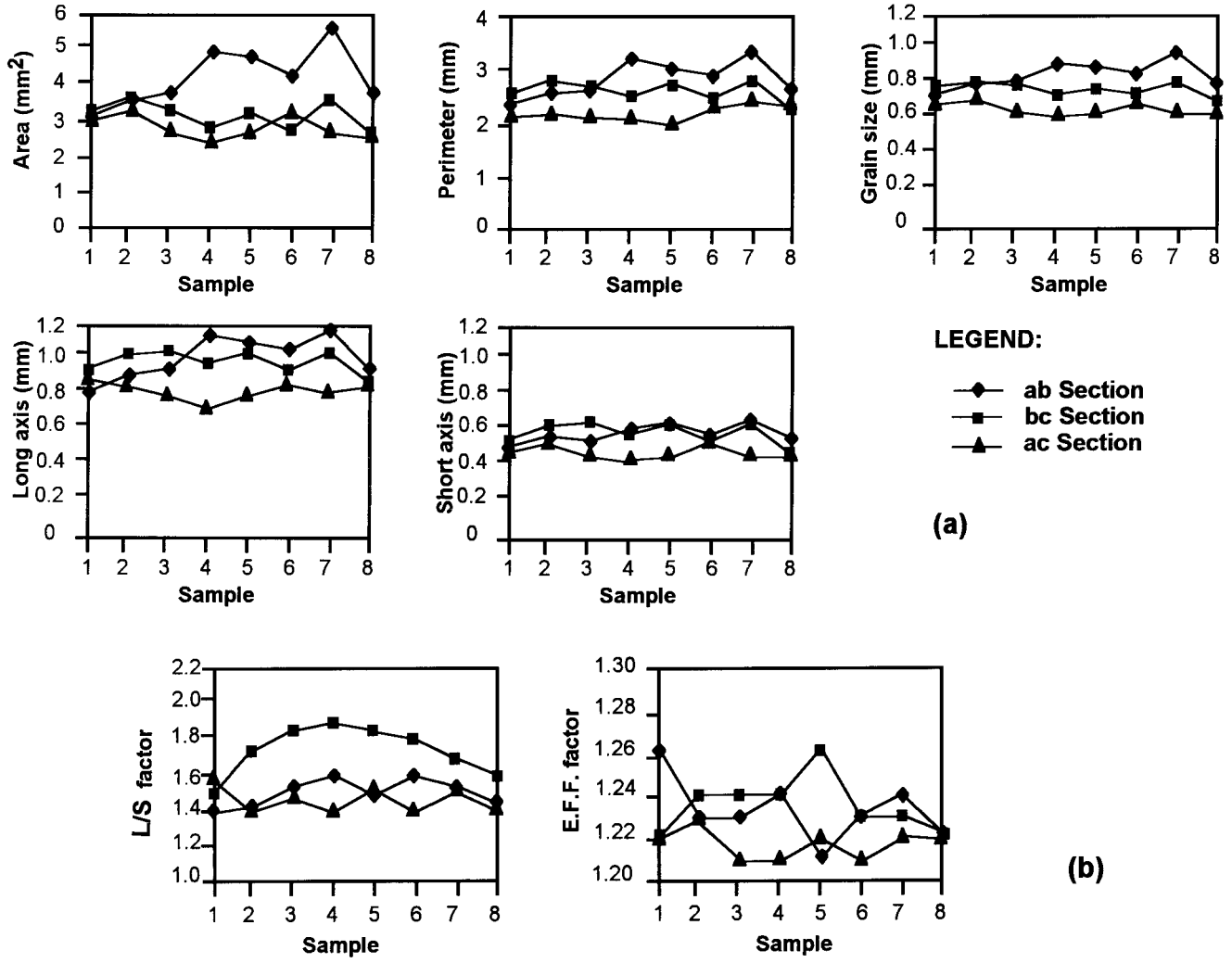

Fig. 9. (a) Plots of the mean values of (A), (P), (L), (S) and grain size, for the three sections measured. (b) Plots of the mean values of the two form factors (L/S and E.F.F.) for the three sections measured.

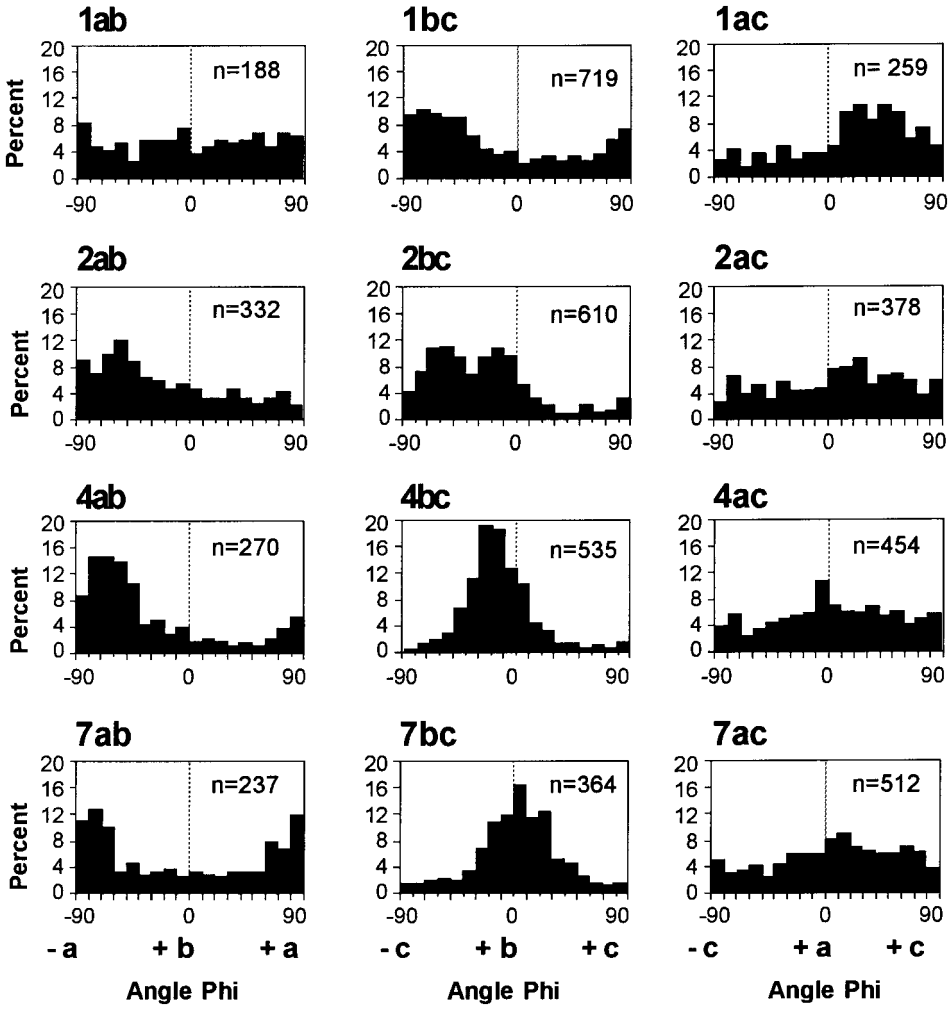

Fig. 10. Histograms of angular values (Phi angle) for the three mutually perpendicular sections. Orientation values of section bc are well grouped around the mean value whereas section ac is poorly oriented. In section ab, only samples 4 and 7 show a clear orientation. Reference axes of the stratigraphic coordinate system are also plotted according to their equivalent angular values.

strain. From the macroscopic point of view, sample M2 can be considered to be on the boundary of the shear zone, and sample M8 in the maximum deformation zone of the shear zone. The angle between the shear walls and bedding varies as it enters the shear zone from 54° in sample M2 to 29° in sample M3, until it is completely parallel to the shear wall in M8 (Fig. 8). Shear strain values in this section of the sheared limb increase from the walls towards the inside of the shear zone from values of 1.5 close to the walls to infinity, only 90 mm away from them (Table 1 and Fig. 5a). The strain increment path plot shows that samples M2 to M8 are on the same strain increment path (Fig. 5b). Therefore, all samples correspond to the deformation of a single reference surface with increasing shear.

The values of the principal strain axes of the ellipse in the *XZ* section were calculated from the shear strain values (Table 1). The relationship between both axes, *X* and *Z*, that is the ellipticity (R), increases from 4 in M3 to values over 100 after M6 (Table 1). The value of the *Y* axis of the finite strain ellipsoid was taken as 1 since we considered plane strain, and therefore, the ellipticity in section *YZ* varies from 2 in sample M3 to infinity in M8.

4.2. Fabric analysis

In order to analyse the fabric variation in the shear zone, samples were collected from the same bed. This bed is separated from the layers above and below by two thin clay layers and consists of three cycles separated by thin layers of enriched sulphate. These cycles are basically formed by small halite grains (approximately 1 mm) and the contacts are mainly of halite–halite since the presence of other minerals is scarce. The main accessory mineral is anhydrite although it is $<1\%$ area. The sulphate enriched and clay layers show millimetre-scale folds and boudins parallel to the fold axis. The total water content in the halite cycles, which is present in the form of intergranular water along grain boundaries, is very low, $<0.1\%$ wt. In accordance with the absence of primary structures in the studied site, water from fluid inclusions or hydrated minerals was

Table 2
Form factor L/S and Phi angle mean values obtained by the bivariant analysis. Note that sample 2 has two angular values in accordance with the two populations described in section bc.

	Section ab			Section bc			Section ac		
Sample	n	Phi	L/S	n	Phi	L/S	n	Phi	L/S
M1	190	81	1.03	719	− 39	1.25	259	39	1.25
M2a	332	− 48	1.20	618	− 60	1.39	381	34	1.04
M2b					− 15				
M3	340	− 63	1.35	605	− 29	1.69	705	9	1.20
M4	277	− 64	1.39	524	− 17	1.65	454	5	1.10
M5	342	− 72	1.30	467	− 4	1.73	486	3	1.18
M6	260	− 89	1.41	421	2	1.53	161	39	1.09
M7	237	87	1.27	364	5	1.56	516	27	1.08
M8	160	− 72	1.21	144	12	1.43	190	10	1.05

not detected. However, small cubic and/or prismatic hopper crystals are abundant in the upper salt member in other areas of the Cardona Formation (Pueyo, 1975).

In an originally sedimentary halite rock, grain shape and size would be conditioned by the presence of primary structures (hoppers from 0.1 mm to a few centimeters or chevron crystals). Therefore, the absence of primary structures raises the question as to whether the observed grain size distribution reflects the original or the recrystallized grain size, or a mixture of both (Hardie et al., 1983). The coexistence of two different grain size populations, due to a size increase or decrease of the original grain size by recrystallization, would be reflected in a frequency distribution of variables such as grain area or the L/S form factor and would be detected by the presence of more than one population. In addition, because salt grains have a short strain memory and recrystallize easily, a detailed quantitative 2-D morphological fabric analysis can provide valuable insights as to how grain populations are organised. Here, this analysis was performed in the two main cycles of halite (intermediate and upper cycles) from the samples.

4.3. Quantitative morphological 2-D analysis

4.3.1. Grain size (2-D)

In this paper, (A), (P), (L), (S) were taken as data sets, which give complementary information to the grain size. The mean values of these parameters were grouped in sections and are shown in Fig. 9a. The mean grain size is included to allow comparison with the other variables. Section **ab** (parallel to the plane defined by the bedding) has the highest values of all these variables from sample 4 to sample 8. Section **ac** shows the lowest values for all the variables. Section **bc** presents higher values than section **ab** in sample 1 and 2 whereas they are similar in sample 3 and lower for the rest of the samples. Grain size, as defined in methods, shows the same trend as the other variables but the values are intermediate between the long and short axis.

4.3.2. Grain shape (2-D)

Two form factors were calculated: the elongation factor (L/S) and the E.F.F. The mean values were grouped in

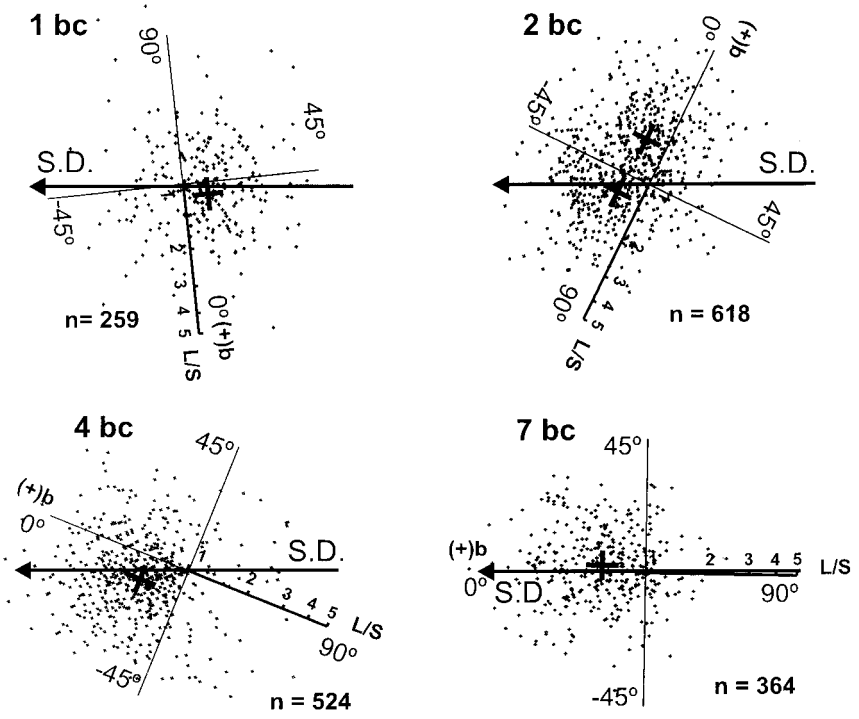

Fig. 11. ln-L/S / 2phi polar plots (according to the projection system described in Elliot (1970)) of samples 1, 2, 4 and 7 in the bc plane of the stratigraphic coordinate system (see text for explanation). The shear plane dip direction (S.D.) has been drawn and taken as a fixed axis whereas the stratigraphic coordinate system is mobile.

Table 3
Magnitude and orientation of the three axis ellipsoid which defines the 3-D mean grain shape. The volume of each sample has also been calculated. L, I and S stand for long, intermediate and short axes respectively whereas a, b and c are the three axes of the startigraphic coordinate system.

Sample		M1	M2a	M2b	M3	M4	M5	M6	M7	M8
Size										
L (mm)		1.096	5.88i	1.85	1.86	1.342	1.132	0.95	1.052	0.953
I (mm)		0.652	0.524	0.55	0.548	0.602	0.648	0.684	0.778	0.604
S (mm)		0.43	0.484	0.482	0.436	0.414	0.438	0.436	0.436	0.424
Volume (mm^3)		1.287	–	2.054	1.862	1.401	1.346	1.495	1.187	1.023
Orientation										
L	a	0.1045	−0.5446	−0.5736	−0.5299	−0.4848	−0.4384	−0.0349	−0.0175	−0.4384
	b	0.7506	0.5612	0.7022	0.7686	0.8364	0.8954	0.9988	0.9974	0.8039
	c	−0.6525	−0.6233	−0.4219	−0.3584	−0.2557	−0.0783	0.0349	0.0697	0.0939
I	a	0.7314	−0.8387	−0.6691	−0.848	−0.8746	−0.8988	−0.891	−0.8746	−0.8572
	b	−0.4988	−0.3428	−0.6983	−0.5094	−0.4704	−0.4367	−0.0158	0.0254	−0.3767
	c	−0.4651	0.4233	−0.2542	0.1461	0.1173	−0.0382	−0.4537	−0.4841	−0.3513
S	a	0.6691	−0.0349	−0.4695	−0.0698	−0.0175	−0.0698	−0.454	−0.4067	−0.2756
	b	0.4368	−0.7542	0.1381	0.3898	0.2756	0.0522	−0.0466	−0.0637	−0.2326
	c	0.6012	−0.6557	0.8721	0.9183	0.9611	0.9962	0.8898	0.9113	0.9327
Shape										
	L / I	1.68	-	3.36	3.39	2.23	1.75	1.39	1.35	1.58
	I / S	1.52	1.08	1.14	1.26	1.45	1.48	1.57	1.78	1.42

sections and are shown in Fig. 9b. Section **bc** shows the highest values and it is the most sensitive to the L/S factor. Values increase from samples 1 to 3, remaining constant to sample 6, and then decrease to sample 8 to values close to sample 1. Section **ab** shows a similar trend but has lower values than section **bc.** Section **ac** is the least sensitive to this factor. Values of E.F.F. are similar in all sections ranging from 1.21 to 1.26. Since for an ellipse with L/S ratio of 2:1 would give a value of E.F.F. of 1.054, the E.F.F. values obtained indicate a moderate degree of rugosity of the grains.

4.3.3. Orientation (2-D)

Histograms of the Phi angular values (Fig. 10) for section **bc** and **ab** show that the orientation values in each sample are well grouped around the mean value whereas for section **ac** they are poorly oriented and more widely dispersed. Section **bc** is the best oriented, except for sample 8 in which the values are not so well grouped around the mean value (Fig. 10). The mean orientation varies from 39° dipping to the north and at a low angle to the shear direction in sample 1, to values parallel to the (+) **b** axis in samples 6 and 7 (Table 2). Nevertheless, sample 2 is an exception and shows two maxima separated by 45°, one close to the maximum of sample 3 and the other closer to the +**b** axis. In section **ab**, the biggest rotation occurs from sample 1 to sample 2. From sample 3 on, they progressively orientate to the (+) **b** axis.

4.3.4. Bivariant analysis (2-D) L/S / Phi method

The mean values of L/S and Phi angle obtained by this method are shown in Table 2. These data are referred to the stratigraphic coordinate system. In all sections, data are dispersed although a tendency as a group can be inferred. Only the results from section **bc**, which is the most sensitive, are shown here (Fig. 11).

In section **bc**, the geometry of the cloud can be estimated from the density distribution of measurements. In Sample 1, this geometry is subcircular and has a mean value that is not related to the shear zone direction. In sample 2, points are distributed around two clusters: the first is located around high negative values close to the shear zone direction and the second has low negative angles (close to sample 1). From samples 3 to 8 the geometry of the cloud is elliptical around the mean angle. The dispersion of the points increases slightly in samples 6 to 8.

In sections **ab** and **ac** (Table 2), the L/S values, which are lower than those in the section **bc**, tend to be grouped close to the mean angle defining a subcircular geometry. The range of L/S values is similar for all Phi values. Only samples 3 to 5 show higher values of L/S for angular values close to the **b** axis.

In short, the most highly sensitive section to morphological changes, due to the elongated shape and orientation of the grains, is section **bc** (Miralles and Sans, 1996), while **ac** is the least sensitive. Nevertheless, it is not always evident which is the best 2-D section beforehand. When the tectonic framework is well constrained a 2-D mophological analysis can be more easily planned, but if the tectonic framework is not well established, then a 3-D analysis has to be carried out. Moreover, when grains are elongated, different shapes can have the same elliptical section (Russ, 1986) and therefore a 3-D analysis is needed to determine the grain shape. A good 3-D shape analysis is calculated from the information obtained from more than two oriented sections.

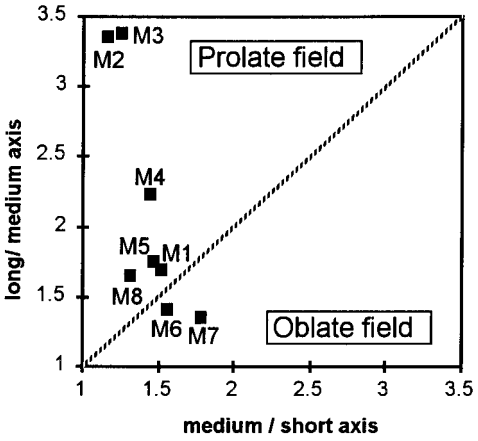

Fig. 12. Distribution of the 3-D calculated grain shape ellipsoids in a ellipsoid-axes-ratio diagram. Most of the samples are in the prolate field and only M6 and M7 are in the oblate field.

4.4. Quantitative morphological 3-D analysis

The resulting 3-D parameters of the grain shape ellipsoid for each sample are given in Table 3. The orientation of the three axes refers to the stratigraphic coordinate system. All samples have a representative unique ellipsoid, except sample 2. Because of the 2-D angular results, it was considered convenient to build two mean grain shape ellipsoids, for sample 2, so as to define its 3-D grain morphology.

4.4.1. Grain size (3-D)

The short axis length was constant from sample 1 to sample 8, except for a slight increase in sample 2. The medium axis length showed small variations, with an increasing tendency from sample 2 up to sample 7. The long axis length underwent the same evolution as the

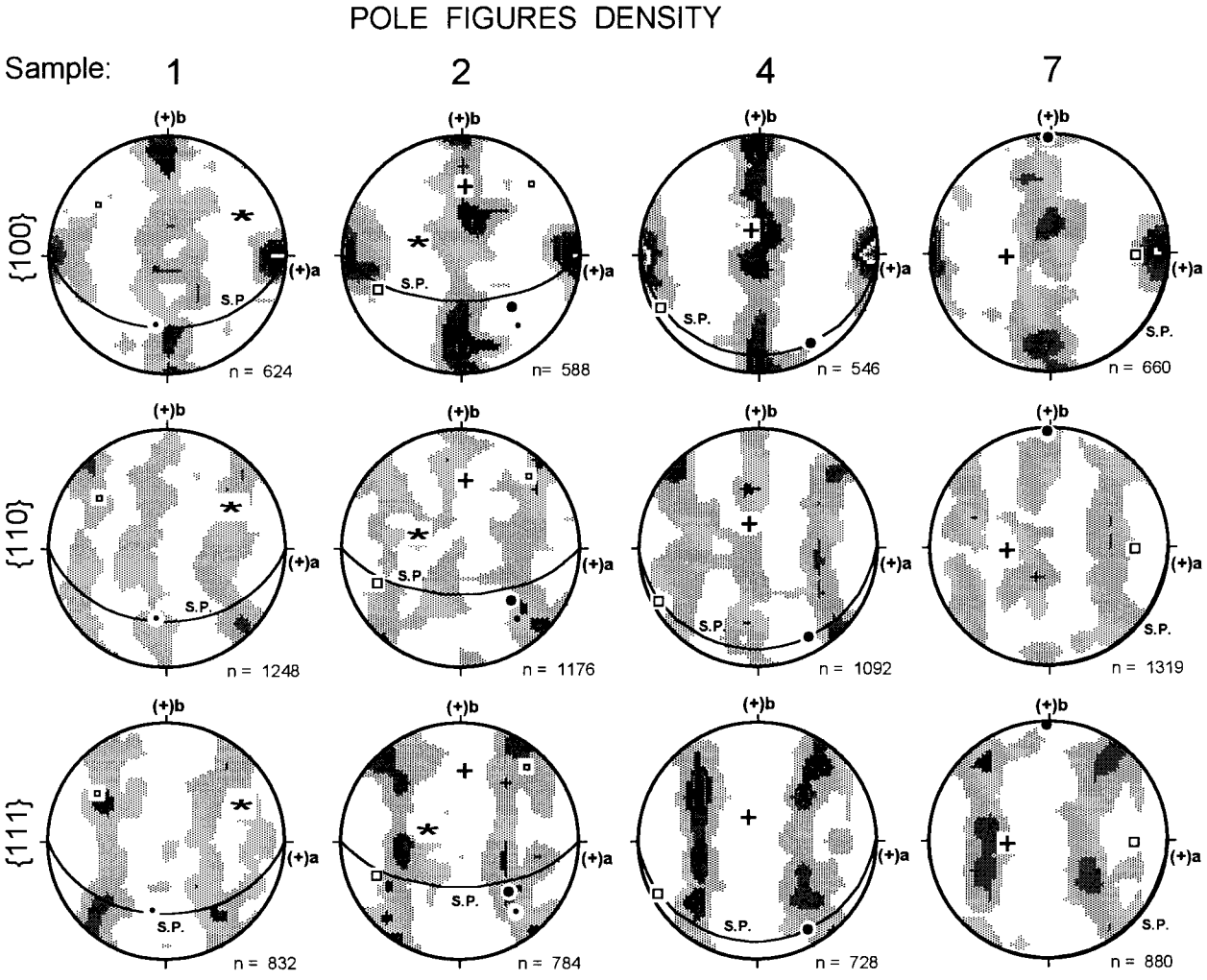

Fig. 13. Pole density figures {100}, {110} and {111} of samples 1, 2, 4 and 7. Data is plotted in the lower-hemisphere equal area projection in which intervals are 1% per 1% area. Data has been rotated and plotted on to the ab plane of the stratigraphic coordinate system since textures are better visualised in this plane. The three grain shape ellipsoid axes have been overprinted (see Fig. 8 for legend). The shear plane (S.P.) is plotted as a great circle. The textures show a main maximum quasi parallel to the fold axis and a girdle along the bc plane and perpendicular to the a axis.

volume change and it is clearly the axis that determines the ellipsoid grain size.

4.4.2. Grain shape (3-D)

The axis relationship (Fig. 12) of most of the samples (1 to 5 and 8) lies in the prolate ellipsoid field. Only samples 6 and 7 lie in the oblate field. Nevertheless, in both fields the ratios are less than 2 and only samples 2 to 4 show a larger ratio.

4.4.3. Orientation (3-D)

In the samples studied the grain shape ellipsoids have two different orientations. The first is related to the cleavage developed in the folds and is present in samples 1 and 2, while the second is related to the shear zone and is present in samples 2 to 8. In sample 1, which is located on the northern limb of the fold and which is not affected by the shear, the long axis of the shape ellipsoid dips to the NW and is subparallel to the fold axial plane. This grain shape ellipsoid might correspond to the cleavage plane. In sample 2, which is located on the southern limb of the fold and at the boundary of the shear zone, two grain shape ellipsoids with different orientations are present. The M2a ellipsoid has a long axis orientation dipping to the NE that could, as in sample 1, correspond to the cleavage plane. The M2b ellipsoid corresponds to a new grain population that grows with the long axis, parallel to the shear plane and the short axis that is perpendicular to it. This orientation of the grain shape ellipsoid is very similar to the orientation of the grain shape ellipsoids in samples 3 to 8. From samples 3 to 5 the long axis progressively becomes parallel with the shear direction and the intermediate axis is also contained in the shear plane. From samples 6 to 8 the intermediate axis is no longer contained in the shear plane and has a misorientation of 25°. This misorientation occurs at the same time as the L/S factor decreases. In sample 8, the long axis also has a misoriention of 20° with respect to the shear plane, which could be explained by the loss of orientation of the Phi angle for section **bc** and the lower values of L/S factor.

In short, the change in the dimensions of the axes results in a volume change in the shape ellipsoids. In samples 2 and 3 (which are located at the boundary of the shear zone), the shape ellipsoids have a larger volume (150%) than in sample 1. However, those samples (4 to 8) which are strongly influenced by the shear zone have a similar volume to sample 1. Grain elongation has been described in many experimental studies in shear conditions as well as grain size increase due to grain boundary migration by dynamic recrystallization (Chester, 1988; Knapp et al., 1987; Ross et al., 1987; Fransen, 1993). Moreover, grain size reduction has been observed with increasing shear strain (Ross et al., 1987; Knapp et al., 1987) by polygonization. However, neither of the experimental conditions that account for grain size increase and reduction can be directly compared with the initial fabrics or deformation conditions of the natural samples studied here. Nevertheless, the grain volume increase in the samples studied is difficult to be explained only by intracrystalline process by dislocation-creep and for this reason we suggest that processes of dynamic recrystallization by mass-transfer might have also taken place.

4.5. Crystallographic preferred orientations

Data were collected in the **bc** thin sections to allow direct comparison with the morphological features since this is the most sensitive section to morphological changes. However, here we present data in the section **ab** as it was in this plane that the different submaxima were more clearly visible. (Fig. 13). All samples exhibit a similar crystallographic preferred orientation pattern. Pole figures of {100} planes show a main maximum almost parallel to the fold axis (**a** axis) and a girdle along the **bc** plane and perpendicular to the **a** axis. The main maximum is asymmetric with respect to the **a** axis because the poles have a larger dip angle to the **c** axis. The girdle, which indicates that there is a degree of freedom in the orientation of the {100} planes, shows different submaxima that cannot be explained by crystal symmetry and cannot be related to any morphological orientation. Therefore, these results indicate that the family of the {100} planes is strongly oriented and perpendicular to the fold axis. Moreover, in samples 4 and 7 one of the maxima in the girdle developed perpendicular to the fold axis is approximately parallel to the short axis of the grain shape ellipsoid. The {100} planes achieve an orientation that can be related to a tectonic direction whereas {110} and {111} are not directly connected to any structural feature of the rock. Nevertheless, to confirm there was no relation with these other two family planes and to permit a better comparison with morphological orientations the {110} and {111} pole figures were calculated from the original data. The pole figures of {110} planes show three low density girdles. Two of them are located at around 45° of the **bc** plane whereas the third is quasi parallel to it. The poles of {111} planes show two better defined girdles at high dip angles with several submaxima along them. In these pole figures, no maxima around the **a** axis or a relationship with the shear zone direction are observed. Nevertheless, in sample 1 the short and intermediate axes lie on the density girdles of the which do not have any direct relationship with the shear zone direction or the orientation of the {110} and {111} pole figures.

This preferred orientation of the {100} planes indicates that there is significant crystallographic control in the orientation of the crystals which, is consistent with dislocation creep processes. In this case, the slip system that usually works in halite at low temperatures, namely $\{110\}\langle 1\bar{1}0\rangle$, could be the main operating system.

Similar patterns were described in Kern and Richter (1985) in the Asse salt dome (Germany) measured on the schistosity plane. Further reports (Carter and Hansen, 1983) also showed a similar texture pattern for Lyons bedded salt

(Carey Mine, Kansas) but the projection plane here was related to the core axis and any comparison with a geological structure is difficult to establish. Other results from naturally deformed samples, obtained by neutron diffraction (Ertel et al., 1987), show a {100} texture pattern for a structure sampled in the Bleicherode mine whereas in the stronger plastically deformed Werra region, they found a {110} texture. It was concluded that the {100} texture does not fit the rock salt layering and does not follow the fold geometry in the perturbation zone of Zielitz mine. The discrepancy between their {100} texture and the {110} texture of experimental work reported by Kern and Richter (1985) in experimental work was attributed to recrystallization processes. On the other hand, patterns (Muehlberger and Clabaugh, 1968) obtained from the macroscopic folds of two Gulf Coast Domes are referred to the axial planes. Their patterns C and F of Fig. 5 of {100} pole figures show similar relationship as our patterns between the crystallographic maxima and the axial plane. Nevertheless, in their work there is a lack of detailed data on the morphological features of the salt grains. Schwerdtner (1968) suggested that slip system $\{110\}\langle 1\bar{1}0\rangle$ followed by annealing recrystallization might account for the fabrics observed in natural rock salt by Muehlberger and Clabaugh (1968).

4.6. Relationship between the strain ellipsoid and the 3-D morphological and crystallographic fabrics

The relationship between fabrics (crystallographic preferred orientations and morphological features) and macrostructure has been well established for high grade metamorphic terrain with quartz. Such analyses have been carried out in the metamorphic areas in which the macrostructure is difficult to analyse and where the strain ellipsoid cannot be obtained directly from the orientation of the folds since their axes are perpendicular and/or parallel to the stretching direction. Salt deforms at a much lower temperature and at lower stress values than quartz to give similar geometric structures. The fact that only a few studies have been conducted on the relationship between mesostructure and fabrics in these sediments is due to the scarce outcropping of salt structures, the cubic properties of the halite and the facility of rock-salt to obliterate the previous fabric, providing therefore, only the record of the last strain increment. Nevertheless, the importance of the evaporitic rocks at levels where deformation is localised has stimulated research on highly strained anhydrites in thin detachment levels in the Alps, Jura and Antalya (Malavielle and Ritz, 1989; Jordan et al., 1990; Marcoux et al., 1987). In such cases, because fold axes are curved, microstructures, as well as the crystallographic fabrics of the anhydrite, have to be studied in order to obtain reliable information on the strain ellipsoid.

Nevertheless, when studying halite fabrics the question is whether the shape and dimensions of the grain shape ellipsoid are related to the strain ellipsoid. Although many authors have done a straightforward correlation (Larsen and Lagoni, 1984), in this work, we observed that the correlation is by no means so straightforward. Two fundamental aspects have to be compared: the orientation of both ellipsoids and their dimensions. The orientation of the grain shape ellipsoid runs parallel to the strain ellipsoid after a deformation of $\gamma = 1.6$. For values close to $\gamma = 1.6$ two fabrics are superimposed in terms of grain shape elongation: one is related to fold development and the other is related to the shear zone.

The analysis of the evolution of grain shape ellipsoid dimensions is more complex. We shall look at this evolution in two parts, the first for values of $\gamma \leq 1.6$ in which the grain shape ellipsoid shows an increase in volume and the second for values of $\gamma \geq 1.6$ in which there is a volume reduction. During grain volume increase, an elongation of the grains occurs along the long axis, whereas the intermediate and short axes remain fairly constant (see values in Table 3). This elongation is proportional to the elongation of the strain ellipsoid long axis. Nevertheless, the grain shape ellipsoid undergoes an increase in volume, which cannot be related to the calculated strain ellipsoid, because as the macrostructural data show the strain ellipsoid is plane strain. Above $\gamma = 1.6$, the strain ellipsoid elongates with increasing strain, whereas the grain shape ellipsoid becomes smaller in volume and less elongated. In particular, the long axis of the grain shape ellipsoid is shortened whereas the intermediate and short axes remain fairly constant. Therefore, although the changes in orientation and dimensions of the grain shape ellipsoid are genetically related to the deformation in the shear zone, there is no direct relationship between the strain and grain shape ellipsoids for values $\gamma \geq 1.6$.

According to the depth and the position at which samples were taken, we can assume that the temperature during deformation was no higher than 80–100°C. At this temperature, the most favourable slip system would have been $\{110\}\langle 1\bar{1}0\rangle$, since families $\{100\}\langle 011\rangle$ and $\{111\}\langle 1\bar{1}0\rangle$ are six or seven times stronger at this temperature (Wenk et al., 1989). Although, given the textures, the slip system $\{110\}\langle 1\bar{1}0\rangle$ could have been operative in all samples, the grain volume increase cannot only be explained by this mechanism. Therefore, tectonically controlled mass-transfer processes were probably active during the first stages of deformation. This is in agreement with theoretical calculations from experimental data (Carter et al., 1990) that predict that mass-transfer processes take place in nature, especially when grain size is as small as 1 mm. Fluid-enhanced grain boundary diffusional creep (Urai et al., 1986; Spiers et al., 1990) can occur with very small amounts of water. The amount of water measured in the studied samples was very low ($<0.1\%$), similar to water contents reported in diapirs (Knauth and Kumar, 1981; de las Cuevas and Pueyo, 1995; Carter et al., 1993). However, in other less tectonised areas of the Cardona Formation this type of salt has a relevant presence of brine-rich fluids related to primary fluid inclusions (hopper crystals) (Pueyo, 1975;

Rosell and Pueyo, 1997; Miralles, 1999). The fluid inclusions of these structures could have constituted a potential supply of water, and therefore have played an important role in the deformation mechanism during the initial stages.

Unlike the rapid spatial changes in morphological fabrics, crystallographic preferred orientations remain constant showing a strong {100} texture, near parallel to the fold axis (**a** axis of the previously defined stratigraphic coordinate system. See Figs. 7 and 13). This preferred orientation is already present in sample 1, and is rotated together with bedding but not modified in the samples inside the shear zone (samples 4 and 7), suggesting that this texture is a prior characteristic. This orientation might respond to the regional shear and shortening undergone by the detachment level.

5. Conclusions

1. Morphological fabrics in naturally deformed small grain size halite (1 mm) show rapid spatial changes, which requires a very careful and close sampling of the structures to evaluate the orientation and dimensions of the grain shape ellipsoid.
2. The 3-D grain shape ellipsoid is parallel to the strain ellipsoid after $\gamma = 1.6$ because a new grain population forms in the tectonic favourable orientation. For values of γ close to 1.6 two grain populations coexist: one lies subparallel to the fold axial plane reflecting the cleavage associated with the fold development and the other lies parallel to the shear direction related to the new grain population.
3. For values of $\gamma > 12$ only the long axis of the grain shape ellipsoid has a good clustering around the shear direction together with a decrease in the L/S factor. For values of $\gamma > 55$ even the long axis starts to lose its good clustering.
4. The dimensions of the grain shape ellipsoid do not provide information about the dimensions of the strain ellipsoid. Grains undergo volume changes, increase for values $\gamma < 2.9$ and decrease for higher values, but in all cases the dimensions of the short and intermediate axes of the grain shape ellipsoid remain nearly constant.
5. Crystallographic fabrics show a constant preferred orientation with respect to bedding. This indicates that the crystallographic fabric is achieved prior to the formation of the shear and that this process does not modify the main trend of the crystallographic fabric. Therefore, during the formation of the shear, the contribution of crystal plasticity (dislocation glide) must be small relative to the total deformation which suggests fluid assisted mass transfer as the main deformation mechanism (consistent with lack of crystallographic preferred orientation).
6. The intracrystalline deformation mechanism coherent with the crystallographic structure and the measured texture is that of the $\{110\}\langle 1\bar{1}0\rangle$ slip system. Grain volume increase cannot be explained by this mechanism alone and, therefore, mass-transfer processes must have taken place.

Acknowledgements

This work has been partially funded by the C.E.E. contract FI-1W-0235-E (TT) in the R + D programme on management and storage of radioactive waste-Part B. H.A.W. (High Active Waste) developed for ENRESA. Additional support was provided by the CIRIT projects GRQ 94-1049 and 1996SGR-0070, and the project 1997SGR-0073 of the Geodinàmica and Anàlisi de Conques group. We would like to thank Súria K S.A. for their help in the underground sampling and supply of information. We are grateful to Jordi Carreras for his thorough revision of the manuscript and comments. David Durney for fruitful discussion and for setting up the computer L/S/phi routines and Juan Jose Pueyo for his overview of the Catalan Potash Basin. Finally, we espress our gratitude to the Serveis Cientificotècnics from the Universitat de Barcelona for their help in the image analysis. The stereographic projections have been performed with the R. Allmendinger Stereonet v. 4.9 program. Review comments by M Brandon and C. Peach are greatly appreciated.

References

Ayora, C., Taberner, C., Pierre, C., Pueyo, J.J., 1995. Modelling the sulfur and oxygen isotopic composition of sulfates through a halite-potash sequence: Implications for the hydrological evolution of Upper Eocene Southpyrenean Basin. Geochimica et Cosmochimica Acta 59, 1799–1808.

Burliga, S., 1996. Kinematics within the Klodawa salt diapir, Central Poland. In: Alsop, G.I., Blundell, D.J., Davison, I. (Eds.). Salt Tectonics. Geological Society Special Publication 100, pp. 11–21.

Busquets, P., Ortí, F., Pueyo, J.J., Riba, O., Rosell, L., Sáez, A., Salas, R., Taberner, C., 1985. Evaporite deposition and diagenesis in the saline (potash) Catalan Basin, Upper Eocene. In: Milá, D., Rosell, J. (Eds.). 6th European Regional Geology Meeting (IAS), Excursion Guidebook, pp. 13–59.

Carreras, J., 1975. Determinación de las relaciones angulares y de la deformación por cizalla, para cizallamientos en materiales con una heterogeneidad planar. Acta Geológica Hispánica 10, 141–145.

Carreras, J., García, A., 1982. Quartz of c-Axis fabric variation at the margins of a shear zone developed in schists from cap de Creus (Spain). Acta Geológica Hispánica 17, 137–149.

Carter, N.L., Heard, H.L., 1970. Temperature and rate dependent deformation of halite. American Journal of Science 269, 193–249.

Carter, N.L., Hansen, F.D., 1983. Creep of rocksalt. Tectonophysics 92, 275–333.

Carter, N.L., Kronenberg, A.K., Ross, J.V., Wiltschko, D.V., 1990. Control of fluids on deformation of rocks. In: Knipe, R.J., Rutter, E.H. (Eds.). Deformation Mechanisms, Rheology and Tectonics. Geological Society Special Publication 54, pp. 1–13.

Carter, N.L., Horseman, S.T., Russell, J.E., Handin, J., 1993. Rheology of rocksalt. Journal of Structural Geology 15, 1257–1271.

Cashman, K., Marsh, B., 1988. Crystal size distribution (CSD) in rocks and

the kinetics and dynamics of crystallization. Contributions to Mineralogy and Petrology 99, 292–305.
Chester, F.M., 1988. The brittle-ductile transition in a deformation-mechanism map for halite. Tectonophysics 154, 125–136.
Davis, J.C., 1986. Statistics and Data Analysis in Geology. John Wiley and Sons, New York.
de las Cuevas, C., Pueyo, J.J., 1995. The influence of mineralogy and texture in the water content of rock salt formations. Its implication in radioactive waste disposal. Applied Geochemistry 10, 317–327.
Elliot, D., 1970. Determination of finite strain and initial shape from deformed elliptical objects. Geological Society of American Bulletin 81, 2221–2236.
Ertel, A., Kämpf, H., Betzl, M., 1987. Texture investigations of natural rock salt using neutron diffraction. Geologica Carpathica 38, 3–17.
Fransen, R.C.M.W., 1993. Rheology of synthetic rocksalt. Ph.D. thesis, University of Utrecht.
Hardie, L.A., Lowenstein, T.K., Spencer, R.J., 1983. The problem of distinguishing between primary and secondary features in evaporites, Sitxth International Symposium on Salt (I), 11-39.
Jordan, P., Noack, T., Widmer, T., 1990. The evaporite shear zone of the Jura Boundary Thrust-New evidence from Wisen well (Switzerland). Eclogae Geologicae Helvetica 83, 525–542.
Kern, H., 1977. Preferred orientation of experimentally deformed limestone marble, quartzite and rock salt at different temperatures and states of stress. Tectonophysics 39, 103–120.
Kern, H., Richter, A., 1985. Microstructures and textures in evaporites. In: Wenk, H.R. (Ed.). Preferred Orientation in Deformed Metals and Rocks: An introduction to Modern Texture Analysis. Academic Press, London, pp. 317–333.
Knapp, S.T., Friedman, M., Logan, J.M., 1987. Slip and recrystallization of halite gouge in experimental shear zones. Tectonophysics 135, 171–183.
Knauth, L.P., Kumar, M.B., 1981. Trace water content of salt in Louisiana salt domes. Science 213, 1005–1007.
Koyi, H., 1998. The shaping of salt diapirs. Journal of Strucutral Geology 20, 321–338.
Kupfer, D.H., 1968. Relationship of internal to external structure of salt domes. In: Braunstein, J., O'Brien, G.D. (Eds.). Diapirism and Diapirs. Memoir of the American Association of Petroleum Geologist 8, pp. 79–89.
Larsen, J., Lagoni, P., 1984. Zechstein salt Denmark; Salt research project EFP-81, Vol 3: Fabric analysis of domal rock salt. Geological Survey of Denmark Series C 1, 100.
Malavielle, J., Ritz, J.F., 1989. Mylonitic deformation of evaporites in décollements: examples from the southern Alps, France. Journal of Structural Geology 11, 583–590.
Marcoux, J., Brun, J.P., Burg, J.P., Burg, J.P., Ricou, L.E., 1987. Shear structure in anhydrite at the base of thrust sheets (Antalya, Southern Turkey). Journal of Structural Geology 9, 555–561.
Miralles, L., Sans, M., 1996. Fábrica de rocas salinas en una zona de cizalla (anticlinal de Súria, Barcelona). Geogaceta 20, 763–766.
Miralles, L., 1999. Estudi de la fàbrica en roques d'halita. El cas de la Conca Potàssica Sudpirinenca. Ph.D. thesis, University of Barcelona.
Muehlberger, W.R., Clabaugh, P.S., 1968. Internal structure and petrofabrics of Gulf Coast salt domes. In: Braunstein, J., O'Brien, G.D. (Eds.), Diapirism and Diapirs. Memoir of the American Association of Petroleum Geologist 8, 90–99.
Peel, F.J., Travis, C.J., Hossack, J.R., 1995. Genetic structural provinces and salt tectonics of the Cenozoic offshore U.S. Gulf of Mexico: A preliminary analysis. In: Jackson, M.P.A., Roberts, D.G., Snelson, S. (Eds.), Salt tectonics: a global prespective, Memoir of the American Association of Petroleum Geologist 65, pp.153-175.
Pinto, V., Casas, A., 1996. An interactive 2D and 3D gravity modeling program for IBM-Compatible personal computers. Computers and Geosciences 22, 535–546.
Pueyo, J.J., 1975. Estudio petrológico y geoquímico de los yacimientos potásicos de Cardona, Súria, Sallent (Barcelona, España). Ph.D. thesis, University of Barcelona.
Ramsay, J.G., 1967. Folding and Fracturing of Rocks. McGraw-Hill, New York.
Ramsay, J.G., Hubert, M.I., 1987. The Techniques of Modern Structural Geology. Folds and Fractures, 2. Academic Press, London.
Rosell, L., Pueyo, J.J., 1997. Second marine evaporitic phase in the South Pyrenean foredeep: The Priabonian Potash Basin. In: Busson, G., Schreiber, B. Ch. (Eds.). Sedimentary deposition in rift and foreland basins in France and Spain (Paleogene and Lower Neogene). Columbia University Press, pp. 358–387.
Ross, J.V., Bauer, S.J., Hansen, F.D., 1987. Textural evolution of synthetic anhydrite-halite mylonites. Tectonophysics 140, 307–326.
Russ, J.C., 1986. Practical Stereology. Plenum Press, New York.
Sans, M., Vergés, J., 1995. Fold development related to contractional salt tectonics: southeastern Pyrenean thrust front, Spain. In: Jackson, M.P.A., Robert, D.G., Snelson, S. (Eds.). Salt tectonics: a global perspective. Memoir of the American Association of Petroleum Geologist, 65, pp. 369–378.
Sans, M., Sánchez, A.L., Santanach, P., 1996a. Internal structure of a detachment horizon in the most external part of the Pyrenean fold-and-thrust belt, (N Spain). In: Alsop, G.I., Blundell, D.J., Davison, I. (Eds.). Salt Tectonics. Geological Society Special Publication 100, pp. 65–76.
Sans, M., Muñoz, J.A., Vergés, J., 1996b. Triangle zone and thrust wedge geometries related to evaporitic horizons (southern Pyrenees). Bulletin of Canadian Petroleum Geology 44, 375–384.
Sans, M., 1999. From thrust tectonics to diapirism. The role of the evaporites in the kinematic evolution in the eastern south-Pyrenean front. Ph.D. thesis, University of Barcelona.
Schwerdtner, W.M., 1968. Intragranular glidding in domal salt. Tectonophysics 5, 353–380.
Skrotzki, W., Welch, P., 1983. Development of texture and microstructure in extruded ionic polycrystalline aggregates. Tectonophysics 99, 47–61.
Spiers, C.J., Urai, J.L., Lister, G.S., Boland, J.N., Zwart, H.J., 1986. The influence of fluid-rock interaction on the rheology of salt rock. Nuclear Science and Technology. EUR 10399 EN. Office for Official Publications of the European Communities, Luxembourg.
Spiers, C.J., Schutjens, P.M.T.M., Brzesowsky, R.H., Peach, C.J., Liezenberg, J.L., Zwart, H.J., 1990. Experimental deformation of constitutive parameters governing creep of rocksalt by pressure solution. In: Knipe, R.J., Rutter, E.H. (Eds.). Deformation Mechanisms, Rheology and Tectonics. Geological Society Special Publication 54, pp. 215–227.
Talbot, C.J., Jackson, M.P.A., 1987. Internal kinematics of salt diapirs. American Association of Petroleum Geologist Bulletin 71, 1068–93.
Urai, J.L., Spiers, C.J., Zwart, H.J., Lister, G.S., 1986. Weakening of rock salt by water during long-term creep. Nature 324 (6097), 554–557.
Urai, J.L., Spiers, C.J., Peach, C.J., Franssen, R.C.M.W., Liezenberg, J.L., 1987. Deformation mechanisms operating in naturally deformed halite rock as deduced from microstructural investigations. Geologie en Mijnbouw 66, 165–176.
Vergés, J., Muñoz, J.A., Martínez, A., 1992. South Pyrenean fold-and-thrust belt: role of foreland evaporitic levels in thrust geometry. In: McClay, K.R. (Ed.). Thrust tectonics. Chapman and Hall, pp. 255–264.
Wanten, P.H., Spiers, C.J., Peach, C.J., 1993. Deformation of NaCl single crystals at 0.27 Tm $=$ T $=0.44$ Tm. In: Hardy, H.R., Langer, M., Habib, P. (Eds.). Proceedings of the Third Conference on Mechanical Behaviour of Saltt, Trans. Tech. Publ, , pp. 103–114.
Wawersik, W.R., Zeuch, D.H., 1986. Modelling and mechanistic interpretation of creep of rock salt below 200°C. Tectonophysics 121, 125–152.
Wenk, H.R., Canova, G., Molinari, A., Mecking, H., 1989. Texture development in halite: Comparison of Taylor model and Self-Consistent theory. Acta Metallurgica 37, 2017–2029.